arXiv:1501.00670v1 [cond-mat.mtrl-sci] 4 Jan 2015

# Ferroelectric properties of $RbNbO_3$ and $RbTaO_3$

A. I. Lebedev*
*Physics Department, Moscow State University, Moscow, 119991 Russia*
(Dated: March 3, 2022)

Phonon spectra of cubic rubidium niobate and rubidium tantalate with the perovskite structure are calculated from first principles within the density functional theory. Based on the analysis of unstable modes in the phonon spectra, the structures of possible distorted phases are determined, their energies are calculated, and it is shown that $R3m$ is the ground-state structure of $RbNbO_3$. In $RbTaO_3$, the ferroelectric instability is suppressed by zero-point lattice vibrations. For ferroelectric phases of $RbNbO_3$, spontaneous polarization, piezoelectric, nonlinear optical, electro-optical, and other properties as well as the energy band gap in the LDA and $GW$ approximations are calculated. The properties of the rhombohedral $RbNbO_3$ are compared with those of rhombohedral $KNbO_3$, $LiNbO_3$, and $BaTiO_3$.
DOI: 10.1134/S1063783415020237

PACS numbers: 61.50.Ah, 63.20.dk, 77.84.Ek

The possibility of ferroelectricity in rubidium niobate and rubidium tantalate with the perovskite structure was discussed by Smolenskii and Kozhevnikova[1] and then by Megaw[2] in the early 1950s. In Ref. 1, the authors referred to unpublished data by V.G. Prokhvatilov who detected the tetragonal $RbTaO_3$ phase with $a = 3.92$ Å, $c = 4.51$ Å exhibiting a phase transition near 520 K; in Ref. 2 these data were simply cited. However, further studies have shown that, unlike lithium, sodium, and potassium niobates, $RbNbO_3$ and $RbTaO_3$ crystallize in individual crystal structures with triclinic $P\bar{1}$ symmetry for $RbNbO_3$ and monoclinic $C2/m$ one for $RbTaO_3$[3–5] when prepared at atmospheric pressure. To obtain these materials with the perovskite structure, they should be prepared at high pressures (65–90 kbar).[6] Due to the difficulties in synthesis of $RbNbO_3$ and $RbTaO_3$ with the perovskite structure, the properties of these crystals have been studied very little.

The phase diagrams of $Rb_2O$–$Nb_2O_5$ and $Rb_2O$–$Ta_2O_5$ systems were studied in Ref. 7 and 8. $RbNbO_3$ is formed by the peritectic reaction and decomposes above 964°C.[7] $RbTaO_3$ decomposes above 600°C probably due to the peritectic reaction too.[8] Rubidium-containing ferroelectric materials in the $BaNb_2O_6$–$NaNbO_3$–$RbNbO_3$ system with the tungsten-bronze structure have high electro-optical properties that substantially exceed those of lithium niobate.[9,10] In Ref. 11, the possibility of using rubidium niobate and rubidium tantalate for photoelectrochemical decomposition of water was discussed. In Ref. 12, it was proposed to use the delamination of $RbTaO_3$ structure to produce porous $TaO_3$ nanomembranes with pore sizes of 1.3×0.6 and 1.1×1.1 Å, which can be used for selective filtration of lithium ions.

The lack of knowledge on the properties of compounds under consideration appears, in particular, in contradictory data on the ferroelectric properties of $RbTaO_3$. For example, the existence of the phase transition at 520 K in the tetragonal phase was reported in Ref. 1, whereas the data of Ref. 6 showed that $RbTaO_3$ prepared at high pressure has the cubic perovskite (or close to it) structure. At 300 K, the structure of $RbNbO_3$ is similar to that of the orthorhombic $BaTiO_3$, and the data of differential thermal analysis indicate phase transitions in it at 15, 155, and 300°C.[6]

In this work, the equilibrium structures of $RbNbO_3$ and $RbTaO_3$ were determined from first-principles calculations, and spontaneous polarization, dielectric constant, piezoelectric and elastic moduli, nonlinear optical and electro-optical properties as well as the energy band gaps in the LDA and $GW$ approximations were calculated for these crystals.

The first-principles calculations were performed within the density functional theory using the `ABINIT` software.[13] The exchange–correlation interaction was described in the local density approximation (LDA). The optimized norm-conserving pseudopotentials for Nb, Ta, and O atoms used in these calculations were taken from Ref. 14. The non-relativistic pseudopotential for the Rb atom (electronic configuration $4s^24p^65s^0$) was constructed according to the scheme of Ref. 15 using the `OPIUM` program[16] with the following parameters: $r_s = 1.68$, $r_p = 1.72$, $r_d = 1.68$, $q_s = 7.07$, $q_p = 7.27$, $q_d = 7.07$, $r_{\min} = 0.01$, $r_{\max} = 1.52$, and $V_{\rm loc} = 1.58$ a.u. (for notations, see Ref. 17). The testing of the Rb pseudopotential on the $P\bar{1}$ phase of $RbNbO_3$ and the $C2/m$ phase of $RbTaO_3$, which are stable at atmospheric pressure, showed its sufficiently high quality: the calculated lattice parameters and atomic coordinates in these phases (see Tables I and II) are in good agreement with the experimental data;[3,5] small underestimates of the calculated lattice parameters are characteristic of the LDA approximation used in this work.

The lattice parameters and equilibrium atomic positions in the unit cells were determined from the condition when the residual forces acting on the atoms were below $5{\cdot}10^{-6}$ Ha/Bohr (0.25 meV/Å) in the self-consistent calculation of the total energy with an accuracy better than $10^{-10}$ Ha. The maximum energy of plane waves was 30 Ha for $RbNbO_3$ and 40 Ha for $RbTaO_3$. Integration over the Brillouin zone was performed using a

TABLE I. Calculated lattice parameters and atomic coordinates in $RbNbO_3$ structures.

| Atom | Position | $x$ | $y$ | $z$ |
|---|---|---|---|---|
| Phase $P\bar{1}$ | | | | |
| $a = 5.0816$, $b = 8.3047$, $c = 8.7916$ Å, | | | | |
| $\alpha = 114.0625$, $\beta = 93.3891$, $\gamma = 95.1160°$ | | | | |
| Rb2 | 1$a$ | +0.00000 | +0.00000 | +0.00000 |
| Rb1 | 1$b$ | +0.00000 | +0.00000 | +0.50000 |
| Rb3 | 2$i$ | +0.41251 | +0.70257 | +0.09488 |
| Nb1 | 2$i$ | +0.49674 | +0.28138 | +0.35602 |
| Nb2 | 2$i$ | +0.02746 | +0.51037 | +0.30988 |
| O1 | 2$i$ | +0.10125 | +0.39078 | +0.82160 |
| O2 | 2$i$ | +0.23664 | +0.42747 | +0.50994 |
| O3 | 2$i$ | +0.28650 | +0.71922 | +0.45293 |
| O4 | 2$i$ | +0.29777 | +0.37205 | +0.19910 |
| O5 | 2$i$ | +0.33951 | +0.05579 | +0.27137 |
| O6 | 2$i$ | +0.78420 | +0.27571 | +0.22313 |
| Phase $Pm3m$ | | | | |
| $a = 4.0291$ Å | | | | |
| Rb | 1$a$ | +0.00000 | +0.00000 | +0.00000 |
| Nb | 1$b$ | +0.50000 | +0.50000 | +0.50000 |
| O | 3$c$ | +0.00000 | +0.50000 | +0.50000 |
| Phase $P4mm$ | | | | |
| $a = 4.0037$, $c = 4.1592$ Å | | | | |
| Rb | 1$a$ | +0.00000 | +0.00000 | −0.00336 |
| Nb | 1$b$ | +0.50000 | +0.50000 | +0.51818 |
| O1 | 2$c$ | +0.50000 | +0.00000 | +0.47446 |
| O2 | 1$b$ | +0.50000 | +0.50000 | −0.03654 |
| Phase $Amm2$ | | | | |
| $a = 3.9928$, $b = 5.7742$, $c = 5.7960$ Å | | | | |
| Rb | 2$a$ | +0.00000 | +0.00000 | −0.00341 |
| Nb | 2$b$ | +0.50000 | +0.00000 | +0.51447 |
| O1 | 4$e$ | +0.50000 | +0.25496 | +0.22842 |
| O2 | 2$a$ | +0.00000 | +0.00000 | +0.47735 |
| Phase $R3m$ | | | | |
| $a = 4.0571$ Å, $\alpha = 89.8945°$ | | | | |
| Rb | 1$a$ | −0.00308 | −0.00308 | −0.00308 |
| Nb | 1$a$ | +0.51193 | +0.51193 | +0.51193 |
| O | 3$b$ | −0.02115 | +0.48415 | +0.48415 |

TABLE II. Calculated lattice parameters and atomic coordinates in $RbTaO_3$ structures.

| Atom | Position | $x$ | $y$ | $z$ |
|---|---|---|---|---|
| Phase $C2/m$ | | | | |
| $a = b = 6.3396$, $c = 8.0171$, | | | | |
| $\alpha = 86.1031$, $\beta = 93.8969$, $\gamma = 96.8997°$ | | | | |
| Rb1 | 4$i$ | +0.16000 | −0.16000 | +0.73758 |
| Rb2 | 4$g$ | +0.26494 | +0.26494 | +0.00000 |
| Ta1 | 4$h$ | +0.31104 | +0.31104 | +0.50000 |
| Ta2 | 4$i$ | +0.23924 | −0.23924 | +0.30214 |
| O1 | 8$j$ | +0.27303 | +0.04639 | +0.39643 |
| O2 | 8$j$ | +0.54749 | −0.21209 | +0.28704 |
| O3 | 4$i$ | +0.16752 | −0.16752 | +0.08653 |
| O4 | 4$i$ | +0.37705 | −0.37705 | +0.55235 |
| Phase $Pm3m$ | | | | |
| $a = 3.9846$ Å | | | | |
| Rb | 1$a$ | +0.00000 | +0.00000 | +0.00000 |
| Ta | 1$b$ | +0.50000 | +0.50000 | +0.50000 |
| O | 3$c$ | +0.00000 | +0.50000 | +0.50000 |

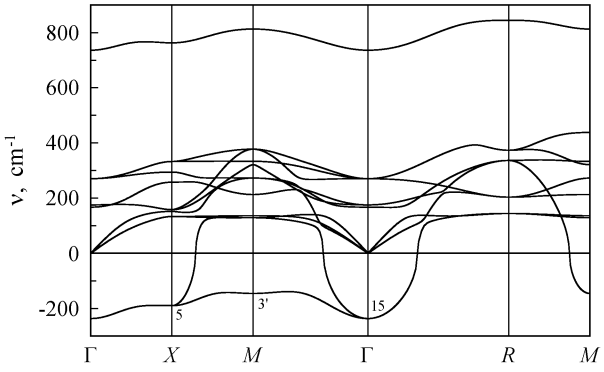



FIG. 1. Phonon spectrum of $RbNbO_3$ in the cubic $Pm3m$ phase. Labels near curves indicate the symmetry of unstable modes.

8×8×8 Monkhorst–Pack mesh. The spontaneous polarization in ferroelectric phases was calculated by the Berry phase method. The phonon spectra, dielectric constants, piezoelectric and elastic moduli were calculated within the density-functional perturbation theory similarly to Ref. 17. Nonlinear optical and electro-optical properties were calculated using the technique described in Ref. 18. All physical properties presented in this work were calculated for the theoretical lattice parameter.

The phonon spectrum of $RbNbO_3$ in the cubic $Pm3m$ phase is shown in Fig. 1. This spectrum contains a band of unstable modes characteristic of ferroelectric chain instability which was first observed in $KNbO_3$.[19] At the center of the Brillouin zone, this mode has the $\Gamma_{15}$ symmetry, is triply degenerate, and describes the ferroelectric distortion of structure. The structures appearing upon condensation of the $X_5$ and $M_3'$ modes are characterized by antiparallel orientation of polarization in neighboring ...–O–Nb–O–... chains.

The energies of all $RbNbO_3$ phases formed upon condensation of the above unstable modes are given in Table III. Among these phases, the $R3m$ phase has the lowest energy. The phonon spectrum calculations for the $R3m$ phase show that the frequencies of all optical phonons at the center of the Brillouin zone and at high-symmetry points at its boundary are positive; the deter-

TABLE III. Relative energies of low-symmetry $RbNbO_3$ phases formed from the cubic perovskite phase upon condensation of unstable phonons, phases with $6H$, $4H$, $9R$, and $2H$ structures, and the $P\bar{1}$ phase prepared at atmospheric pressure (the most stable phase energy is in boldface).

| Phase | Unstable mode | Energy, meV |
|---|---|---|
| $Pm3m$ | — | 0 |
| $P4/nmm$ | $M_3'$ | −31.3 |
| $Pmma$ | $X_5$ | −34.8 |
| $Cmcm$ | $X_5$ | −38.7 |
| $P4mm$ | $\Gamma_{15}$ | −46.5 |
| $Amm2$ | $\Gamma_{15}$ | −57.0 |
| $R3m$ | $\Gamma_{15}$ | **−58.6** |
| $P\bar{1}$ | — | +27.4 |
| $P6_3/mmc$ $(6H)$ | — | +121.4 |
| $P6_3/mmc$ $(4H)$ | — | +334.0 |
| $R\bar{3}m$ $(9R)$ | — | +568.1 |
| $P6_3/mmc$ $(2H)$ | — | +1752 |

TABLE IV. Relative energies of low-symmetry $RbTaO_3$ phases formed from the cubic perovskite phase upon condensation of unstable phonons, phases with $6H$, $4H$, $9R$, and $2H$ structures, and the $C2/m$ phase prepared at atmospheric pressure (the most stable phase energy is in boldface).

| Phase | Unstable mode | Energy, meV |
|---|---|---|
| $Pm3m$ | — | 0 |
| $P4mm$ | $\Gamma_{15}$ | −1.80 |
| $Amm2$ | $\Gamma_{15}$ | −1.87 |
| $R3m$ | $\Gamma_{15}$ | **−1.90** |
| $C2/m$ | — | +38.5 |
| $P6_3/mmc$ $(6H)$ | — | +113.3 |
| $P6_3/mmc$ $(4H)$ | — | +352.2 |
| $R\bar{3}m$ $(9R)$ | — | +589.0 |
| $P6_3/mmc$ $(2H)$ | — | +1839 |

minant and all leading principal minors constructed of elastic moduli tensor components are also positive. This means that the $R3m$ phase is the ground-state structure of $RbNbO_3$. The calculated lattice parameters and atomic coordinates in this phase are given in Table I. As the same sequence of phases as in $BaTiO_3$ is supposed in rubidium niobate with the perovskite structure,[6] the lattice parameters and atomic coordinates in two other ferroelectric phases are also given in this table. The lattice parameters calculated for the orthorhombic $RbNbO_3$ are in good agreement with the experimental data obtained at 300 K ($a$ = 3.9965, $b$ = 5.8360, and $c$ = 5.8698 Å, Ref. 6).

In $RbTaO_3$, the frequency of unstable $\Gamma_{15}$ phonon in the phonon spectrum (Fig. 2) and the energy gain resulting from the transition to ferroelectric phases (Table IV) are rather low; so it is necessary to additionally

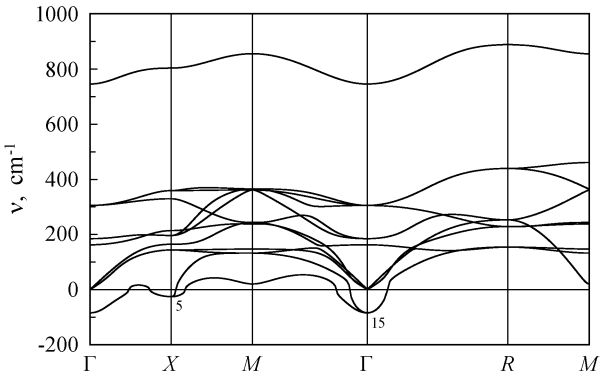



FIG. 2. Phonon spectrum of $RbTaO_3$ in the cubic $Pm3m$ phase. Labels near curves indicate the symmetry of unstable modes.

test the stability of the ferroelectric distortion with respect to zero-point lattice vibrations. For this purpose, we used the technique proposed in Ref. 20. The energy gain resulting from the transition from the $Pm3m$ phase to the $R3m$ phase is $E_0$ = 1.90 meV and the unstable phonon frequency at the Γ point in the $Pm3m$ phase is $\nu = 84$ cm$^{-1}$. As the energy ratio $h\nu/E_0 = 5.51$ exceeds the critical value of 2.419 obtained in Ref. 20, the energy of the lowest vibrational state in a two-well potential appears above the upper point of the energy barrier separating the potential wells, and the ferroelectric ordering is suppressed by zero-point vibrations. Therefore, the only stable phase of $RbTaO_3$ with the perovskite structure is the cubic phase. The calculated lattice parameter of this phase is given in Table II; its value is in satisfactory agreement with the experimental data ($a$ = 4.035 Å, Ref. 6).

It is known that the formation of phases with hexagonal $BaNiO_3$ (polytype $2H$), hexagonal $BaMnO_3$ (polytype $4H$), hexagonal $BaTiO_3$ (polytype $6H$), and rhombohedral $BaRuO_3$ (polytype $9R$) structures is characteristic of $ABO_3$ perovskites with the tolerance factor $t > 1$, and the studied compounds belong to this class. Our calculations showed that the energies of these phases for both rubidium compounds are appreciably higher than the cubic phase energy (Tables III and IV). These results explain why it was impossible to observe the transition of $RbNbO_3$ to the hexagonal structure[6] upon heating, by analogy to that occurring in $BaTiO_3$. The high energies of these phases, in particular, the $2H$ phase, are probably caused by larger sizes and strong electrostatic repulsion of $Nb^{5+}$ ions which occupy face-sharing octahedra in these structures.

We consider now some properties of ferroelectric $RbNbO_3$. The calculated polarization in $RbNbO_3$ is 0.46 C/m$^2$ in the $P4mm$ phase and 0.50 C/m$^2$ in the $Amm2$ and $R3m$ phases; these values slightly exceed the calculated polarization in the same phases of $KNbO_3$ (0.37, 0.42, and 0.42 C/m$^2$, respectively). The static di-

TABLE V. Nonzero components of the piezoelectric tensor $e_{i\nu}$ ($C/m^2$) and tensors of the second-order nonlinear optical susceptibility $d_{i\nu}$ and the linear electro-optic effect $r_{i\nu}$ (pm/V) in rhombohedral phases of $RbNbO_3$, $KNbO_3$, $LiNbO_3$, and $BaTiO_3$.

| Coefficient | $RbNbO_3$ | $KNbO_3$ | $LiNbO_3$ | $BaTiO_3$ |
|---|---|---|---|---|
| $e_{11}$ | −3.0 | −4.2 | −2.4 | −4.0 |
| $e_{15}$ | +4.8 | +6.8 | +3.5 | +7.3 |
| $e_{31}$ | +2.4 | +2.3 | +0.1 | +3.5 |
| $e_{33}$ | +2.9 | +3.1 | +1.1 | +5.1 |
| $d_{11}$ | +12.7 | +11.9 | +2.3 | +4.4 |
| $d_{15}$ | −23.6 | −21.9 | −11.5 | −16.1 |
| $d_{31}$ | −23.6 | −21.9 | −11.5 | −16.1 |
| $d_{33}$ | −29.4 | −27.3 | −37.4 | −31.1 |
| $r_{11}$ | −12.8 | −17.7 | −5.6 | −13.7 |
| $r_{15}$ | +27.6 | +39.2 | +17.1 | +43.3 |
| $r_{31}$ | +18.0 | +23.9 | +10.1 | +25.3 |
| $r_{33}$ | +30.1 | +40.6 | +27.3 | +48.9 |

electric tensor in the $R3m$ phase is characterized by two eigenvalues: $\varepsilon_{\parallel}^{0} = 21.1$ and $\varepsilon_{\perp}^{0} = 35.8$; the optical dielectric tensor eigenvalues are $\varepsilon_{\parallel}^{\infty} = 5.31$ and $\varepsilon_{\perp}^{\infty} = 5.91$. In the cubic phase, the elastic moduli are $C_{11} = 412$, $C_{12} = 84$, and $C_{44} = 102$ GPa; the bulk modulus is $B = 193.5$ GPa. The nonzero components of the tensors of piezoelectric effect $e_{i\nu}$, second-order nonlinear optical susceptibility $d_{i\nu}$, and linear electro-optic (Pockels) effect $r_{i\nu}$ in the $R3m$ phase of rubidium niobate are compared with the corresponding properties of other rhombohedral ferroelectrics in Table V. We can see that the piezoelectric moduli in rhombohedral $RbNbO_3$ (as well as in its other polar phases) are slightly lower than in $KNbO_3$. The nonlinear optical coefficients in $RbNbO_3$ exceed the corresponding values in $KNbO_3$, although the $d_{33}$ value in rubidium niobate is slightly lower than in lithium niobate. As for the electro-optical properties, in rhombohedral $RbNbO_3$ they are slightly lower than in $KNbO_3$, but are notably superior to those of lithium niobate. In the orthorhombic phase (stable at 300 K), nonlinear optical properties of $RbNbO_3$ are comparable to those of the same phase of potassium niobate: for example, the $d_{33}$ modulus is −30.8 pm/V in $RbNbO_3$ and −30.4 pm/V in $KNbO_3$.

In cubic $RbTaO_3$, the optical dielectric constant is $\varepsilon_\infty = 5.58$. The static dielectric constant can be estimated only in the rhombohedral phase as ∼140. The elastic moduli in cubic rubidium tantalate are $C_{11} = 466$, $C_{12} = 91.5$, and $C_{44} = 120$ GPa; $B = 216$ GPa. The piezoelectric moduli, second-order nonlinear optical susceptibility, and electro-optical coefficients in the cubic phase are zero.

An unexpected result of our calculations is that in both studied compounds the $P\bar{1}$ and $C2/m$ phases which can be prepared at atmospheric pressure are metastable. This result is probably caused by an effective lattice contraction which always exists in the LDA calculations. The fact that the specific volume of the $Pm3m$ phase is noticeably smaller than that of $P\bar{1}$, $C2/m$, $P6_3/mmc$, and $R\bar{3}m$ phases suggests that under pressure the cubic perovskite phase will be the most stable one. To estimate the maximum value of the actual effective pressure, the lattice parameters and atomic positions in the $C2/m$ structure of rubidium tantalate were calculated for different pressures and it was shown that the unit cell volume equal to the experimental one at 300 K can be obtained at an isotropic pressure of −24.7 kbar. At this pressure, the enthalpy of the $C2/m$ phase becomes lower than that of $Pm3m$ by ∼230 meV, i.e., becomes consistent with the experimental data. At the above-mentioned negative pressure, the ratio $h\nu/E_0$ determining the stability of the ferroelectric phase in $RbTaO_3$ becomes equal to 1.90, i.e., it is slightly lower than the critical value of 2.419. However, if we take into account that the above negative pressure is obviously overestimated because it includes the thermal expansion effect, we can suppose that, even taking into account the systematic error in the LDA lattice parameter determination, rubidium tantalate will remain cubic up to the lowest temperatures.

The conclusion that $RbTaO_3$ is an incipient ferroelectric in which the ferroelectric ordering is suppressed by zero-point vibrations agrees with the data of Ref. 6, but contradicts the data of Ref. 1 in which the phase transition near 520 K was reported. We suppose that tantalum-enriched phases (in particular, with the tungsten-bronze structure[8]) could be formed in rubidium tantalate samples discussed in Ref. 1 because of the low temperature of the peritectic reaction, and this could result in the observed anomaly.

In Ref. 11, the possibility of using various oxides with the perovskite structure, in particular $RbNbO_3$ and $RbTaO_3$, for development of photoelectrochemical solar cells was discussed. We calculated the band gap $E_g$ in these compounds both in the LDA approximation and in the $GW$ approximation that takes into account many-body effects (the technique of the latter calculations was analogous to that used in Refs. 21–23). In the LDA approximation, $E_g^{\mathrm{LDA}} = 1.275$ eV in cubic $RbNbO_3$ when the spin–orbit coupling is neglected; in $P4mm$, $Amm2$, and $R3m$ phases, $E_g^{\mathrm{LDA}}$ is 1.314, 1.869, and 2.137 eV, respectively. In cubic $RbTaO_3$, $E_g^{\mathrm{LDA}} = 2.175$ eV when the spin–orbit coupling is neglected. The valence band extrema in the cubic phase of both compounds are at the $R$ point of the Brillouin zone, whereas the conduction band extrema are at the Γ point. The calculations using the technique of Ref. 23 yield the spin–orbit splitting of the conduction band edge $\Delta_{SO} = 0.111$ eV for $RbNbO_3$ and $\Delta_{SO} = 0.400$ eV for $RbTaO_3$; the spin-orbit splitting of the valence band edge is absent. After correction for the conduction band edge shift ($\Delta_{SO}/3$), the LDA values of $E_g$ that take into account the spin–orbit coupling are 1.238, 1.277, 1.832, 2.100, and 2.042 eV for four $RbNbO_3$ phases and for cubic $RbTaO_3$, respectively.

In the *GW* approximation, the band gap when the spin–orbit coupling is neglected is $E_g^{GW} = 2.403$, 2.616, 3.291, and 3.609 eV, respectively in cubic, tetragonal, orthorhombic, and rhombohedral $RbNbO_3$ and 3.302 eV in cubic $RbTaO_3$. If the spin–orbit coupling is taken into account, these values decrease to 2.366, 2.579, 3.254, 3.572, and 3.169 eV, respectively. The obtained values of $E_g$ are appreciably smaller than those calculated in Ref. 11 for cubic phases (3.4 eV for $RbNbO_3$ and 4.3 eV for $RbTaO_3$).

Some authors who studied rubidium niobate and rubidium tantalate have noticed their sensitivity to humidity. Evidently, this can be a serious obstacle for practical applications of these materials. However, we would like to note that this property is inherent to phases prepared at atmospheric pressure and having loose structures whose specific volume is 26–28% larger than that of the perovskite phase. In Ref. 8, it was suggested that the effect is due to intercalation of water molecules into the loose structures, rather than to hydrolysis of these compounds. The possibility of preparing $RbTaO_3$ by hydrothermal synthesis[24] and the low rate of $RbTaO_3$ ion exchange in HCl during its delamination[12] support this idea. This suggests that the considered compounds with the perovskite structure can be quite stable to humidity.

In summary, the present calculations of $RbNbO_3$ and $RbTaO_3$ properties and their comparison with the properties of other ferroelectrics show that rubidium niobate is an interesting ferroelectric material with high nonlinear optical and electro-optical properties, and rubidium tantalate is an incipient ferroelectric.

The calculations presented in this work were performed on the laboratory computer cluster (16 cores).

This work was supported by the Russian Foundation for Basic Research, project no. 13-02-00724.

* swan@scon155.phys.msu.ru


1. G. A. Smolenskii and N. V. Kozhevnikova, Dokl. Akad. Nauk SSSR **76**, 519 (1951).
2. H. D. Megaw, Acta Cryst. **5**, 739 (1952).
3. M. Serafin and R. Hoppe, J. Less-Common Metals **76**, 299 (1980).
4. M. Serafin and R. Hoppe, Angewandte Chem. **90**, 387 (1978).
5. M. Serafin and R. Hoppe, Z. Anorg. Allg. Chem. **464**, 240 (1980).
6. J. A. Kafalas, in *Proc. of 5th Materials Research Symposium* (National Bureau of Standards Special Publication 364, 1972) pp. 287–292.
7. A. Reisman and F. Holtzberg, J. Phys. Chem. **64**, 748 (1960).
8. H. Brusset, H. Gillier-Pandraud, M. Chubb, and R. Mahé, Mater. Res. Bull. **11**, 299 (1976).
9. D. F. O'Kane, G. Burns, E. A. Giess, B. A. Scott, A. W. Smith, and B. Olson, J. Electrochem. Soc. **116**, 1555 (1969).
10. G. Burns, E. A. Giess, and D. F. O'Kane, "New ferroelectric materials and process of preparation," U.S. Patent No. 3,640,865 (08 Feb. 1972).
11. I. E. Castelli, D. D. Landis, K. S. Thygesen, S. Dahl, I. Chorkendorff, T. F. Jaramillo, and K. W. Jacobsen, Energy Environ. Sci. **5**, 9034 (2012).
12. K. Fukuda, I. Nakai, Y. Ebina, R. Ma, and T. Sasaki, Inorg. Chem. **46**, 4787 (2007).
13. "The ABINIT code is a common project of the Université Catholique de Louvain, Corning incorporated and other contributions, `http://www.abinit.org/`".
14. A. I. Lebedev, Phys. Solid State **52**, 1448 (2010).
15. A. M. Rappe, K. M. Rabe, E. Kaxiras, and J. D. Joannopoulos, Phys. Rev. B **41**, 1227 (1990).
16. "Opium—pseudopotential generation project," `http://opium.sourceforge.net/`.
17. A. I. Lebedev, Phys. Solid State **51**, 362 (2009).
18. M. Veithen, X. Gonze, and P. Ghosez, Phys. Rev. B **71**, 125107 (2005).
19. R. Yu and H. Krakauer, Phys. Rev. Lett. **74**, 4067 (1995).
20. A. I. Lebedev, Phys. Solid State **51**, 802 (2009).
21. A. I. Lebedev, Phys. Solid State **54**, 1663 (2012).
22. A. I. Lebedev, J. Alloys Comp. **580**, 487 (2013).
23. A. I. Lebedev, Phys. Solid State **56**, 1039 (2014).
24. D. Gompel, M. N. Tahir, M. Panthofer, E. Mugnaioli, R. Brandscheid, U. Kolb, and W. Tremel, J. Mater. Chem. A **2**, 8033 (2014).